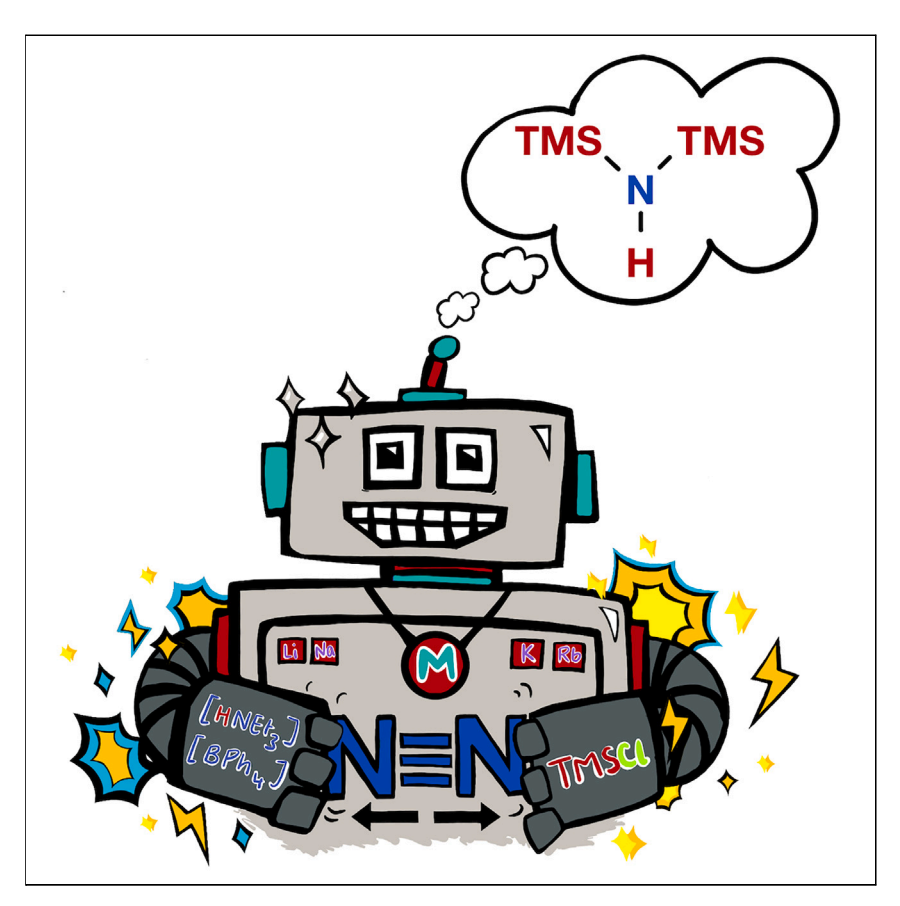


#### **Article**

# Catalytic reduction of dinitrogen to silylamines by earth-abundant lanthanide and group 4 complexes



The low-energy conversion of atmospheric dinitrogen to amines is a grand challenge and could bring food and energy justice to many. For decades, chemists targeting homogeneous catalysts for this, citing biology as inspiration, have focused on electron-rich d-block complexes. Now, metallacycles formed from cheap, earth-abundant f-block and group-4 complexes with bridging phenolates can trap dinitrogen and moderate its reduction and functionalization. Studies demonstrate the importance of the metal-ligand architecture and cooperativity in controlling for unusual bis(substituted) nitrogen reduction products.

Anthony Wong, Francis Y.T. Lam, Matthew Hernandez, ..., R. David Britt, Nikolas Kaltsoyannis, Polly L. Arnold

pla@berkeley.edu

#### Highlights

Ambient conversion of  $N_2$  to bis(silyl)amines ( $N_2RR$ ) by electropositive metal aryloxides

First rare-earth-metal-complex-mediated N<sub>2</sub>RR catalysts

First zirconium-complexmediated N<sub>2</sub>RR catalyst

Robust, recyclable Ti-based  $N_2RR$  catalyst with highest TON to date

Wong et al., Chem Catalysis 4, 100964 May 16, 2024 © 2024 Elsevier Inc. All rights reserved. https://doi.org/10.1016/j.checat.2024.100964







#### **Article**

# Catalytic reduction of dinitrogen to silylamines by earth-abundant lanthanide and group 4 complexes

Anthony Wong,<sup>1</sup> Francis Y.T. Lam,<sup>1</sup> Matthew Hernandez,<sup>1</sup> Jaden Lara,<sup>1</sup> T. Michael Trinh,<sup>1</sup> Rory P. Kelly,<sup>1</sup> Tatsumi Ochiai,<sup>1</sup> Guodong Rao,<sup>2</sup> R. David Britt,<sup>2</sup> Nikolas Kaltsoyannis,<sup>3</sup> and Polly L. Arnold<sup>1,4,\*</sup>

#### **SUMMARY**

Dinitrogen is a challenging molecule to reduce to useful products under ambient conditions. The range of d-block metal complexes that can catalyze dinitrogen reduction to ammonia or tris(silyl) amines under ambient conditions has increased recently but lacks electropositive metal complexes, such as those of the f-block, which lack filled d-orbitals that would support classical binding modes of N<sub>2</sub>. Here, metallacyclic phenolate structures with lanthanide or group 4 cations can bind dinitrogen and catalyze its conversion to bis(silyl)amines under ambient conditions. The formation of this unusual product is controlled by metallacycle sterics. The group 4 complexes featuring small cavities are most selective for bis(silyl)amine, while lanthanide complexes and the solvated uranium(IV) congener, with larger cavities, can also make a conventional tris(silyl)amine product. These results offer new catalytic applications for plentiful titanium and more earth-abundant members of the lanthanides that are also less toxic than many base metals used in catalysis.

#### INTRODUCTION

One of the most interesting challenges in homogeneous bond activation chemistry is dinitrogen ( $N_2$ ). The strong  $N \equiv N$  bond (bond dissociation free energy [BDFE] = 945 kJ mol $^{-1}$ ) and large highest occupied molecular orbital-lowest unoccupied molecular orbital gap (10.82 eV) result in a high activation energy barrier and significant energy input requirement for the nitrogen reduction reaction ( $N_2RR$ ). Taking inspiration from nature, electron-rich, mid-d-block complexes $^{2-7}$  have been widely studied for the reductive functionalization of  $N_2$  to ammonia or its protected equivalent tris(trimethylsilyl)amine  $N(SiMe_3)_3$  (Scheme 1A). The number of complexes showing turnover has recently started to increase rapidly. For example, one of the most successful studies to date has focused on developing a family of Mo-based PXP (X = C, N, P) pincer complexes that convert  $N_2$  to  $NH_3$ . Through extensive catalyst optimization involving tuning of both the ligand and the reaction conditions, yields have improved with each generation from 12 equiv of ammonia per Mo atom to thousands, although the most effective catalysis is stoichiometric in  $Sm^{II}$  reductants.

 $N_2RR$  catalysts with Lewis acidic early d-block metals are significantly rarer. A small number of titanium complexes have been reported to effect catalytic reductive functionalization of dinitrogen. <sup>15</sup> In the 1990s, Mori and co-workers reported that the reaction of  $Ti(O^iPr)_4$  with lithium, 45 equiv of  $Me_3SiCl$ , and dinitrogen (1 atm) gave a mixture assumed to contain  $[ClTi=NSiMe_3]$ ,  $[Cl_2Ti-N(SiMe_3)_2]$ , and  $N(SiMe_3)_3$  which could subsequently be converted into benzamide by treatment with HCl. <sup>1</sup> The other previously reported homogeneous titanium  $N_2RR$  catalysts, both supported by the

#### THE BIGGER PICTURE

Small-cavity metallacycles containing two earth-abundant lanthanide, actinide, or group 4 cations catalyze the conversion of ambient, atmospheric N2 to bis(silyl)amines. The reduction of dinitrogen is challenging and has, for a century, been studied with electron-rich d-block metal compounds since conventional f-block metal complexes do not have filled d-orbitals that would enable binding of N2. The metal cations, reductant, and ligand architecture work cooperatively, providing new fundamental information on this important transformation and showing how the nitrogen-binding cavity can be used to control the selective formation of bis(substituted) amines. The development of a new catalyzed reaction using f-block ions teaches us more about these less commonly studied metals. Because this system works in a polar solvent, opportunities to use a green source of electrons, e.g., from solar power, could enable smallerscale amine production from atmospheric nitrogen wherever the sun shines.



### **CellPress**

# Chem Catalysis

chelating, more electron-donating, substituted tris(ethylenediamino)amine (tren) ligand, showed catalytic  $N_2RR$  forming up to 9 equiv of  $NH_3$  or 16.5 equiv of  $N(SiMe_3)_3$  per Ti.  $^{16-18}$ 

Homogeneous  $N_2RR$  catalysts remain limited to d-block metals with the sole exception of our f-block metallacyclic uranium catalyst  $U_2(L)_2$ , 1U,  $^{19}$  where L = the O-donor tetraphenolate [ $\{2-(OC_6H_2-2^{-t}Bu,4-Me)_2CH\}-1,3-C_6H_4\}$ ],  $^{20}$  which was able to catalyze the conversion of ambient  $N_2$  to secondary silylamines in the presence of reductant, weak acid, and  $Me_3SiCl$  electrophile, generating 6.4 equiv of amine per complex (Scheme 1B). Calculations and the characterization of an intermediate containing the  $[N_2H_2]^{2-}$  fragment suggested that the reactive ligand C-H in L facilitates delivery of a proton to the activated  $N_2$  ligand.  $^{19}$  Prior to this, we had shown dinitrogen reduction by  $U^{III}$  centers with monodentate aryloxide or siloxide ligands, but reactions to target the further  $N_2$  reduction needed for N-element bond formation usually results in O-ligand scrambling.  $^{21-23}$ 

The U<sub>2</sub>(L)<sub>2</sub> complex 1U was also the first catalyst to selectively make a secondary amine from catalytic N<sub>2</sub>RR. <sup>19</sup> Our discovery of the uranium catalysis was unexpected since the valence electrons that electron-rich d-block cations use to stabilize N<sub>2</sub> adducts, via back bonding from metal to the unoccupied nitrogen  $\pi$ -orbitals, <sup>24</sup> are not readily accessible to f-block metal cations, whose valence f-orbitals are contracted. The first evidence for N<sub>2</sub> binding in f-block chemistry came from the Sm<sup>II</sup> organometallic complex Cp\*<sub>2</sub>Sm, which exists in a dynamic equilibrium with the formally Sm<sup>III</sup>, reduced dinitrogen adduct  $\{Cp_2^*Sm\}_2(\mu-N_2)$  ( $Cp^*=\eta-C_5Me_5$ ) in toluene solution under an N<sub>2</sub> atmosphere, demonstrating a minimally activated N<sub>2</sub> group.<sup>25</sup> More recently, combining simple Ln<sup>III</sup> complexes with potassium metal or KC<sub>8</sub> under a dinitrogen atmosphere forms complexes containing the N2 dianion in the form  $\{X_2Ln(sol)_n\}_2(\mu-N_2)$  (Ln = Sc, Y, La-Nd, Gd-Tm, Lu; X = bulky monodentate anionic O-, N-, or C-donor ligand, M = K, n = 0-2) and, in some cases, triply reduced  $N_2$  complexes  $[K(sol')][\{X_2Ln(sol)_n\}_2(\mu-N_2)]$  (Ln = Y, Er, and La, Gd–Er, Lu; sol = monodentateor crown-ether or cryptand). <sup>26–33</sup> This new family of complexes upturned 90 years of accepted wisdom by proving that rare earths can bind and reduce dinitrogen, thus transforming conceptualizations of d- and f-orbital participation in bonding. 34,35 Indeed, some of the complexes display remarkable magnetic properties as a result of their unusual electronic structures.<sup>36</sup> However, the only rare-earth complexes that have shown N-element bond formation to date are the methylation of the  $N_2$  trianion in  $[\{X_2Sc\}_2(\mu-N_2)]^{-}$ , which forms a  $(N_2Me_2)^{2-}$  unit, <sup>37</sup> and protonation of the side-on, reduced (N<sub>2</sub>)<sup>3-</sup> yttrium analog with [HNEt<sub>3</sub>][BPh<sub>4</sub>], which forms a crystallographically characterized bridging (N<sub>2</sub>H<sub>2</sub>)<sup>2-</sup> unit.<sup>38</sup>

We considered the most significant discovery of our work in  $N_2RR$  catalysis to be the formation of a secondary amine HN(SiMe<sub>3</sub>)<sub>2</sub> as opposed to the usually observed product N(SiMe<sub>3</sub>)<sub>3</sub>. Here, we show that earth-abundant 4f and group 4 metal congeners of 1U can form metallacyclic catalysts for the conversion of  $N_2$  to bis(silyl)amines at ambient conditions. The THF-solvated f-block complexes, which have larger metallacyclic cavities, can also catalyze the transformation of  $N_2$  to tris(silyl)amines, highlighting the increased flexibility of f-block catalysts compared to the d-block.<sup>39</sup>

#### **RESULTS**

#### Synthesis and structures of the group 4 and lanthanide catalysts

The colorless bis- $Ln^{III}$  metallacycles  $[K_2Ln_2(L)_2(THF)_n]$  1Ln-THF (Ln = Ce, n = 4; Ln = Sm, n = 3) and bis- $M^{IV}$  metallacycles  $[M_2(L)_2]$  1M, M = Ti yellow, Zr colorless) are

<sup>&</sup>lt;sup>1</sup>University of California, Berkeley, and Lawrence Berkeley National Laboratory, Berkeley, CA 94720, USA

<sup>&</sup>lt;sup>2</sup>University of California, Davis, Davis, CA 95616, USA

<sup>&</sup>lt;sup>3</sup>Department of Chemistry, University of Manchester, Oxford Road, Manchester M13 9PL, IJK

<sup>&</sup>lt;sup>4</sup>Lead contact

<sup>\*</sup>Correspondence: pla@berkeley.edu https://doi.org/10.1016/j.checat.2024.100964

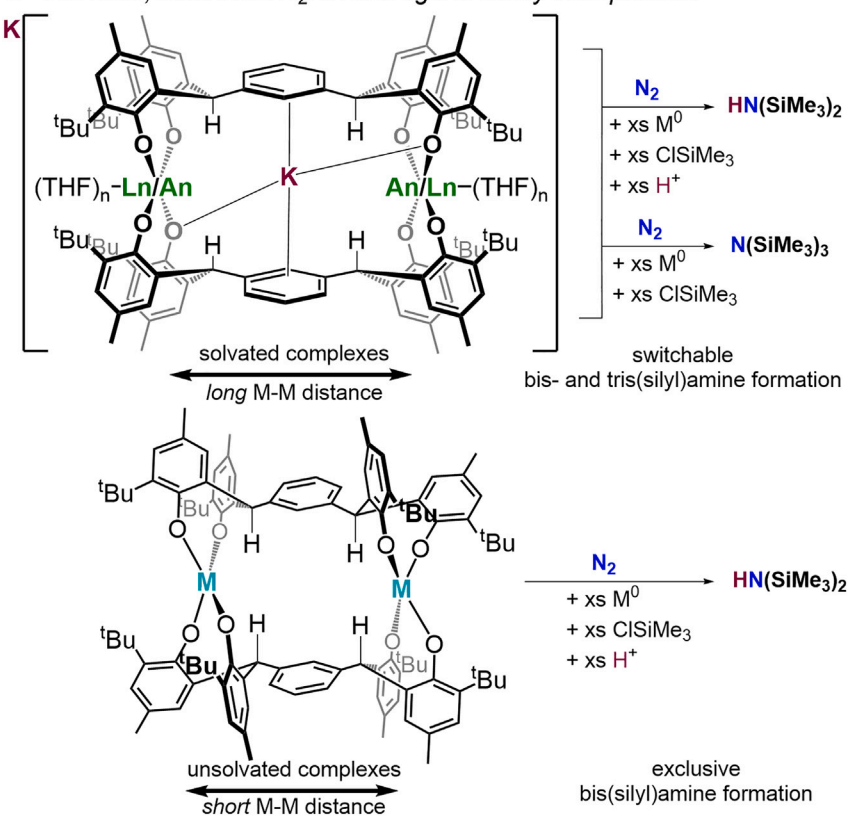
#### Article



A Nitrogen Reduction Reaction (N<sub>2</sub>RR) to silylamines

в previous work

c this work; controlled N<sub>2</sub>RR and ligand cavity manipulation



#### Scheme 1. The $N_2RR$ catalysts 1Ln-THF, 1An, 1U-THF, and 1Ti/Zr

- (A) Generic catalyzed reaction for the conversion of N<sub>2</sub> to tris(silyl)amine.
- (B) Previous work on the unsolvated tetravalent 1U, which has a small metallacyclic cavity, as a catalyst for  $N_2RR$ .
- (C) This work on lanthanide 1Ln-THF and solvated uranium 1U-THF catalysts with larger metallacyclic cavities (top) and unsolvated group 4 complexes 1Ti and 1Zr with smaller cavities



# Chem Catalysis Article

#### Scheme 1. Continued

(bottom). All catalyze the ambient conversion of  $N_2$  to secondary silylamines, and the larger-cavity complexes (1Ln-THF, 1U-THF) also catalyze the ambient conversion of  $N_2$  to tertiary silylamines. Ln = Ce, n = 4; Sm, n = 3; U, n = 4; M = Ti, Zr; xs., excess.

prepared via protonolysis reactions between metal precursors and the tetraphenol  $H_4L$  in THF or arene solvent. The molecules (Scheme 1C) have been fully characterized, including by single-crystal X-ray diffraction (XRD) (see Figures S77–S83 and 1). Complex 1Ti is air stable. Cyclic voltammetry data for THF solutions of 1Ln-THF, 1U-THF, 1Ti, and 1Zr with supporting alkyl ammonium-based electrolytes are shown in Figures S1–S5. The cyclic voltammogram of 1Ti contains two reversible reductions at  $E_{1/2} = -1.91$  V and -2.11 V vs. Fc/Fc<sup>+</sup> assigned as metal-based events. On reduction event that could be assigned to a metal reduction was measurable for the other precatalysts within the electrochemical solvent window, i.e., as far as -3.2 V vs. Fc/Fc<sup>+</sup>.41,42

The relationship between the geometry of the metallacycle pocket and the potential for reactivity within it is of greatest interest. The solid-state structure of 1Sm-THF shows two octahedral Sm centers that form a rectangular cavity through coordination of two anionic aryloxide donors of each tetraanionic L (Figure 1A). The Sm-Sm distance in 1Sm-THF is 9.3830(7) Å, significantly longer than the U-U distances in both the unsolvated 1U (6.5732(5) Å) and the hydrazido adduct  $[K_4U_2(\mu-\eta^2:\eta^2-\eta^2)]$  $N_2H_2$ )(L<sup>-</sup>)<sub>2</sub>] (4.6422(7) Å), which contains the four-electron reduced ( $N_2H_2$ )<sup>2-.19</sup> However, it is similar to the U-U distance in the solvated 1U-THF, 9.3069(7) Å, 19 since the two additional THF ligands on each metal displace the weak U-C close contacts formed with the meta-arene in 1U.19 In addition, there is one potassium counter cation located in the 1Ln-THF cavity with bonds to Ln through two phenolate O atoms and an  $\eta^1$  interaction with the central carbon in the bridging arene of each L; the arenes are co-planar but offset. A second K<sup>+</sup> counter cation is solvated outside the cavity by six THF molecules. The structure of the cerium congener 1Ce-THF is very similar to that of 1Sm-THF (see Figure S80) except for slightly longer Ln-O bonds ( $r_{cov, 6-coord}$ : Ce(III) = 1.15, Sm(III) = 1.098 Å, U(IV) = 1.03 Å).

In contrast, both 1Ti and 1Zr display two tetrahedral metal centers (Figure 1B for Ti) and shorter M–M distances (7.8902(4) Å for 1Ti and 7.8240(9) Å for 1Zr), likely due to their smaller ionic radii of Ti and Zr compared to those of the lanthanides (Figure S83;  $r_{cov, 4-coord}$ : Ti(IV) = 0.56, Zr(IV) = 0.73 Å).

A common feature between 1Ln-THF and 1M (Ln = Ce, Sm; M = Ti, Zr) is that all four benzylic C–H bonds point into the metallacyclic cavity, whereas in 1U and 1U-THF, only two (one from each L) point inwards; the benzylic CH, assigned C7 and C30, in the structure of 1Sm-THF are further from the center of the cavity than they are in 1U by an average of 1.31  $\mathring{\rm A}$ . The distances between the closest benzylic C-H and the midpoint between the two Sm in 1Sm-THF or two Ti in 1Ti are 3.72  $\mathring{\rm A}$  in 1Sm-THF and 3.70  $\mathring{\rm A}$  in 1Ti.

#### Catalytic N<sub>2</sub>RR

The metallacyclic complexes 1Ln-THF, 1U-THF, and 1M are catalysts for the conversion of  $N_2$  to bis(silyl)amine HN(SiMe<sub>3</sub>)<sub>2</sub>; the general reaction involves stirring a THF solution of the catalyst with an excess of potassium metal to provide electrons, excess chlorotrimethylsilane Me<sub>3</sub>SiCl (electrophile), and excess weak acid [HNEt<sub>3</sub>][BPh<sub>4</sub>] together under an ambient  $N_2$  atmosphere for 24 h (Scheme 2A). Reactions of 1Ln-THF, 1U-THF, and 1M were also carried out in the absence of acid to target formation

#### **Article**



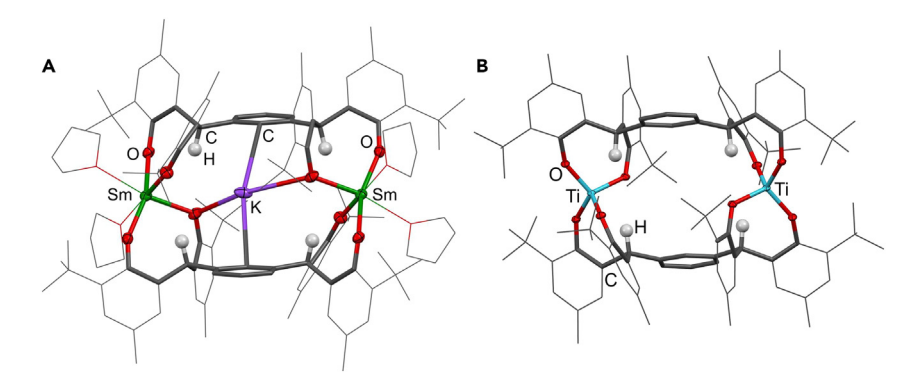


Figure 1. Structure of the N<sub>2</sub>RR catalysts 1Sm-THF and 1Ti

(A) Anion of **1Sm-THF** and (B) **1Ti**. Hydrogen atoms, lattice solvent, and the [K(THF)<sub>6</sub>] counter cation for **1Sm-THF** are omitted for clarity. The inter-lanthanide/group 4 metal cation distances are Sm1–Sm2 = 9.3830(7) Å, Ce1–Ce2 = 9.3706(5) Å, Ti1–Ti2 = 7.8902(4) Å, and Zr1–Zr2 = 7.8241(7) Å (see supplemental information).

of the tris(silyl)amine (Scheme 2B). In THF, 1U is converted to 1U-THF, which is much more catalytically active compared to the unsolvated 1U was in arene solvent. A range of control reactions and reactions under different conditions and with alternative reagents and isotopomers are described in the supplemental information.

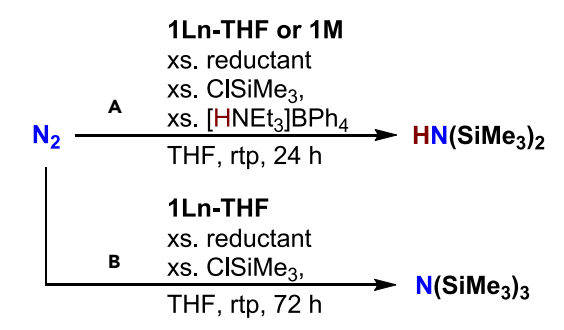
The most informative reactions are outlined in Table 1. Nitrogen reduction products are identified and quantified by <sup>29</sup>Si nuclear magnetic resonance (NMR) spectroscopy and gas chromatography (GC) (Figures S9–S11 and S37–S50), and yields are reported as an average of three runs.

Under an atmosphere of  $N_2$  at room temperature, the complex 1Sm-THF catalytically converts dinitrogen to the bis(silyl)amine HN(SiMe<sub>3</sub>)<sub>2</sub>, forming 3.71  $\pm$  0.62 equiv of amine per binuclear 1Sm-THF complex (Table 1, entry 2). This is the second instance of catalytic  $N_2$  reduction providing a selective route to secondary amine product formation, following 1U. <sup>19</sup> Under the same conditions, 1Ce-THF produces silylamines in close to stoichiometric quantities (Table 1, entry 1), affording a combined 2.1 equiv of bis(silyl)amine and tris(silyl)amine by-product (see below) per molecule of 1Ce-THF. Lastly, 1U-THF generates 20.5  $\pm$  1.7 combined equiv of amine and is a better catalyst than 1U (6.4 equiv of amines in our initial report). <sup>19</sup>

In the absence of weak acid, 1Sm-THF is an even better catalyst for the conversion of  $N_2$  to tris(silyl)amine, making 5.44  $\pm$  0.81 equiv per 1Sm-THF. Yields for 1Ce-THF are substoichiometric (Table 1, entries 6 and 7) unless Rb is used as the reductant partner instead of K (Table 1, entry 4), yielding 2.80  $\pm$  0.48 equiv of tris(silyl)amine. For 1Sm-THF, K is the most effective group 1 metal reductant (Tables 1; Table S1, entries 1–18). 1U-THF also catalyzes the formation of N(SiMe<sub>3</sub>)<sub>3</sub>, yielding 10.1  $\pm$  1.5 equiv of the tris(silyl)amine; this contrasts with the inability of 1U to produce the tris(silyl)amine in arene solvent, which we attribute to the larger cavity of solvated 1U-THF. The precatalyst 1Sm-THF is more active for the synthesis of tris(silyl)amine than bis(silyl)amine because a side reaction with the weak acid takes the active catalyst out of the solution. The reaction of 1Sm-THF with [HNEt<sub>3</sub>][BPh<sub>4</sub>] (8 equiv) in THF shows the release of some H<sub>4</sub>L after 1 h (Figure S55). The group 4 complexes do not release H<sub>4</sub>L, even after prolonged reaction times.

Compound 1Ti gives the highest turnovers for  $N_2RR$  yet reported for any molecular Ti catalyst with combined 35.1  $\pm$  1.4 equiv of amine being produced (Table 1,





Scheme 2.  $N_2RR$  catalyzed by the lanthanide, uranium, and group 4 complexes 1Ln-THF, 1U-THF, and 1M (Ln = Ce, Sm; M = Ti, Zr)

(A) Ambient temperature and pressure formation of  $HN(SiMe_3)_2$  from  $N_2$  catalyzed by the lanthanide metallacycles 1Ln-THF, 1U-THF, or 1M using a group 1 metal reductant, trimethylchlorosilane electrophile, and a weak acid.

(B) The conventional product  $N(SiMe_3)_3$  can be made by 1Ln-THF or 1U-THF if acid is omitted. rtp, room temperature and pressure; xs., excess.

entry 9; Table S2, entry 2). Furthermore, the catalyst longevity of 1Ti was tested by adding further reagent to the post-run catalytic mixture, yielding a combined 84.1 equiv of amine for the four collected runs (Table 1, entry 12; Table S2, entry 11). The two reported homogeneous titanium N2RR catalysts gave up to 9 equiv of NH<sub>3</sub> or 16.5 equiv of N(SiMe<sub>3</sub>)<sub>3</sub> per Ti. <sup>16–18</sup> The heavier Zr metallacycle 1Zr is the first Zr-based N<sub>2</sub>RR catalyst, though it is poorer and less selective than 1Ti, forming  $HN(SiMe_3)_2$  (5.46  $\pm$  0.45 equiv) and  $N(SiMe_3)_3$  (2.74  $\pm$  1.56 equiv) (Table 1, entry 11). Even Ti(OAr)<sub>4</sub> (OAr = OC<sub>6</sub>H<sub>3</sub>-2-<sup>t</sup>Bu-4-Me) supported by monodentate aryloxides can catalyze the formation of bis(silyl)amine in the presence of a 2:1 ratio of silyl electrophile to acid, albeit in poorer yields than 1Ti (see Table 1, entry 13). We considered if the ratio of acid to electrophile might dominate the product selectivity, but others have not seen this selectivity.<sup>39</sup> Therefore, we suggest that the combination of Ti(OAr)4 and potassium counter cations in the reaction mixture can also form a protected space around the Ti-N2 species that gives some selectivity for the bis(silyl)amine. Further, decreasing the fraction of acid below the 2:1 ratio of R<sub>3</sub>Si<sup>+</sup>:H<sup>+</sup> decreases both yield and selectivity for bis(silyl)amine with 1Ti (Table S2, entry 4).

Interestingly, both 1M and 1U are inactive for the catalytic formation of  $N(SiMe_3)_3$  (Table 1, entry 10; Table S2, entry 20). <sup>19</sup> We suggest that this is due to insufficient space in the metallacycle for product turnover. For 1Sm-THF, 1Ti, and 1Zr, K is also the most effective group 1 metal reductant (Table S2, entries 1–24). In all cases studied, sodium as reductant gives little or no turnover for  $N_2RR$ . Replacement of the reductant K with Na for 1 results in substoichiometric yields of the silylamines (e.g., 0.42 equiv of  $HN(SiMe_3)_2$  and 0.43 equiv of  $N(SiMe_3)_3$  for ISm-THF). The replacement of  $IHNEt_3$  salts with other weak acids including  $IHPCy_3$  [CI] and phenol are described in Figure S41 and Table S2 (entries 6 and 8–10).

In the catalytic reactions to form HN(SiMe<sub>3</sub>)<sub>2</sub>, N(SiMe<sub>3</sub>)<sub>3</sub> is a by-product of a secondary reaction between the newly formed HN(SiMe<sub>3</sub>)<sub>2</sub> and K metal to form KN(SiMe<sub>3</sub>)<sub>2</sub>, which reacts with ClSiMe<sub>3</sub>. To demonstrate this, aliquots were removed over the course of different runs, using 1Ti, 1U-THF, or Ti(OAr)<sub>4</sub>, and analyzed by GC. In the 1Ti-catalyzed reaction, the amount of HN(SiMe<sub>3</sub>)<sub>2</sub> increases over the first 9 h (Figure S12) and then plateaus and starts to decrease as the N(SiMe<sub>3</sub>)<sub>3</sub> by-product starts to form (Figure S14). We repeated the kinetic study using the standard conditions, except we replaced [HNEt<sub>3</sub>][BPh<sub>4</sub>] with [DNEt<sub>3</sub>][BPh<sub>4</sub>], and observed a decrease in

Article



Table 1. Catalytic conversion of  $N_2$  to silylamines by metallacycles 1Ln-THF, 1U-THF, and 1M under ambient conditions

Entry	Precatalyst	Reductant (300 equiv) <sup>a</sup>	ClSiMe <sub>3</sub> equiv	[HNEt <sub>3</sub> ][BPh <sub>4</sub> ] equiv <sup>b</sup>	HN(SiMe <sub>3</sub> ) <sub>2</sub> equiv <sup>c</sup>	N(SiMe <sub>3</sub> ) <sub>3</sub> equiv
1	1Ce-THF	K	225	131	1.84	0.26
2	1Sm-THF	K	225	131	$3.71 \pm 0.62$	0
3	1U-THF	K	225	131	$17.5 \pm 1.4$	$2.91 \pm 1.71$
4	1Ce-THF	Rb	300	0	0	$2.80 \pm 0.48$
5	1Sm-THF	Rb	300	0	0	$3.29 \pm 0.22$
6	1Ce-THF	K	300	0	0	1.21
7	1Sm-THF	K	300	0	0	$5.44 \pm 0.81$
8	1U-THF	K	300	0	0	$10.1 \pm 1.5$
9	1Ti	K	225	131	$29.7 \pm 0.9$	$5.35 \pm 0.51$
10	1Ti	K	300	0	0	1.44
11	1Zr	K	225	131	$5.46 \pm 0.45$	$2.74 \pm 1.56$
12 <sup>d</sup>	1Ti	K	225 (4×)	131 (4×)	75.9	8.16
13	Ti(OAr) <sub>4</sub>	K	225	131	16.3 ± 1.0	$2.43 \pm 0.79$

<sup>&</sup>lt;sup>a</sup>Reductant.

the overall rate of formation of H/DN(SiMe<sub>3</sub>)<sub>2</sub>, which may suggest that N–H bond formation/cleavage is involved in the rate-determining step (Figure S13). Analogous kinetic studies with both 1U-THF and Ti(OAr)<sub>4</sub> show the same trend as 1Ti: the bis (silyl)amine product is made early in the reaction, while the tris(silyl)amine product is only produced during later time points (Figures S15 and S16).

### Studies of potential intermediates arising from $N_2$ reduction and reductive dehydrometallation

In the 1U  $N_2RR$  system, we characterized an intermediate containing a doubly reduced and doubly protonated, side-on-bound dinitrogen and demonstrated that the NH in  $HN(SiMe_3)_2$  derives from the benzylic CH group within the metallacycle. We targeted a reduced  $N_2$ -containing complex from the reactions between 1Sm-THF or 1Ti and excess potassium under  $N_2$  (Scheme 3).

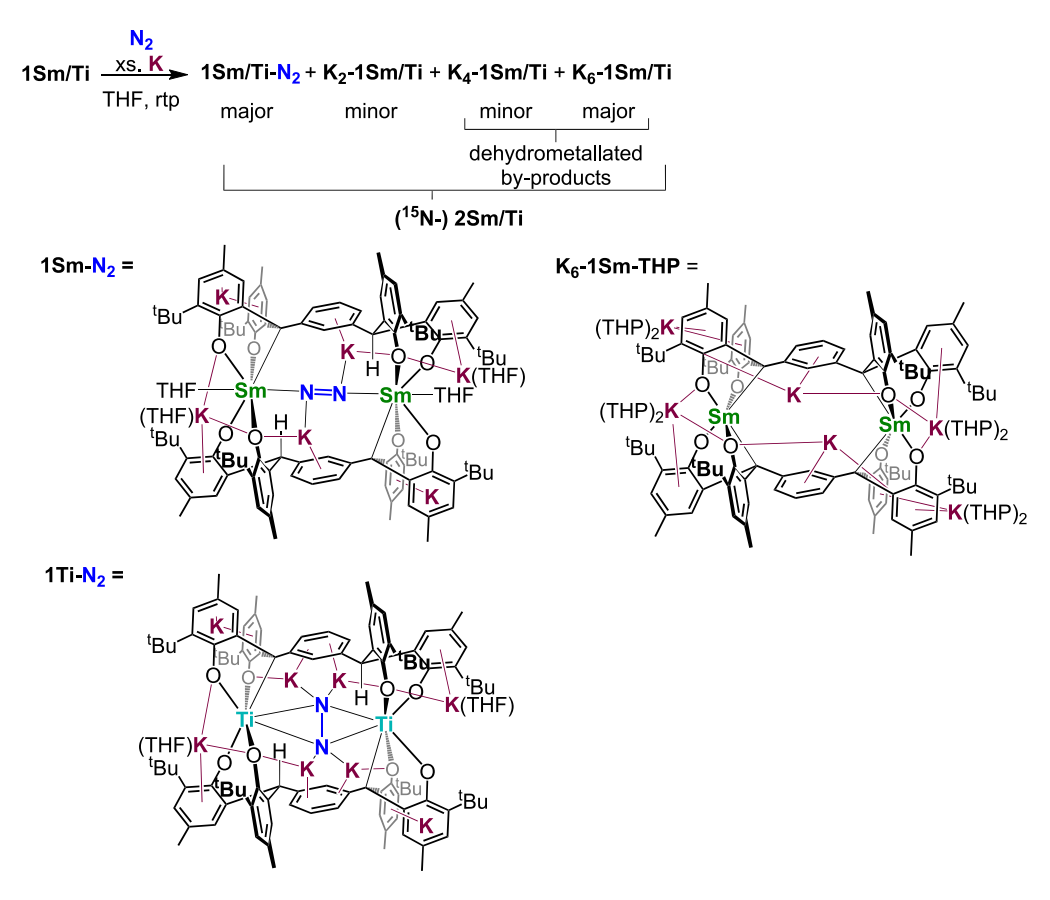
In each case, we isolate a dark red powder that contains a mixture of complexes, denoted 2Sm and 2Ti, respectively, containing a reduced  $N_2$  species and products containing M– $C_{benzylic}$  bonds arising from the deprotonation of one or more ligand benzylic CH groups, i.e., dehydrometallated congeners of 1Sm/Ti. We were unable to isolate pure compounds from the mixture 2Sm due to similar solubilities and extreme air sensitivity but have used isotopomer substitutions and spectroscopies to confirm that around half of the material in each case is a reduced dinitrogen adduct. Analysis (electron-spray ionization mass spectrometry and NMR spectroscopies) of the reduced mixtures 2Sm and 2Ti after quenching with the weak acid [DNEt<sub>3</sub>][BPh<sub>4</sub>] reveals the overall level of dehydrometallation to be around one-quarter of the total ligand benzylic CH groups in each case (Figures S6, S7, S29, S30, and S34–S36).

Complete deprotonation of the benzylic carbons forms  $[K_6(THF)_4M^{III}_2(L^{2-})_2]$   $(K_6-1 Sm/Ti)$  as red-orange  $K_6-1Sm$  or olive green  $K_6-1Ti$ , which we can make independently and have structurally characterized for both M=Sm (as the THP solvate  $[K_6(THP)_8M^{III}_2(L^{2-})_2]$ ) and Ti (supplemental information).  $L^{2-}$  is the hexaanionic

<sup>&</sup>lt;sup>b</sup>Catalysis results with other weak acids are in the supplemental information.

<sup>&</sup>lt;sup>c</sup>Yields quoted for all these complexes are per molecule rather than per Ln/M; average of 3 or more runs. <sup>d</sup>Additional reagent added to recycled, post-run **1Ti** catalyst showing catalyst longevity; product yield reported for the four collected runs.





Scheme 3. Reduction of 1Sm-THF or 1Ti under dinitrogen in the absence of electrophile and acid

The products are reduced,  $N_2$ -containing and dehydrometallated mixtures denoted **2Sm** or **2Ti**, and line drawings of proposed structures of **1Sm-N<sub>2</sub>**, **1Ti-N<sub>2</sub>**, and the structurally characterized THP solvate of  $K_6$ -**1Sm**,  $K_6$ -**1Sm**-THP. The solid-state structures of  $K_6$ -**1Sm**-THP,  $K_4$ -**1Zr**, and the three  $K_n$ -**1Ti** (n = 2, 4, 6) are shown in the supplemental information. THP, tetrahydropyran.

ligand [ $\{2-(OC_6H_2-2^{-t}Bu-4-Me)_2C\}-1,3-C_6H_4\}$ ]. The respective M–M distances in 1 Sm/Ti vs.  $K_6$ -1 Sm/Ti are 9.3830(7) vs. 6.8395(7) Å for Sm and 7.8902(4) vs. 6.9919(12) Å for Ti. We expect that these metallations that reduce the cavity size disfavor  $N_2$  binding since the M–C<sub>benzylic</sub> bonds reduce the void volume: only the complexes without Ti–C<sub>benzyl</sub> bonds (1Ti and  $K_2$ -1Ti) are capable of binding  $N_2$  upon further reduction (see Scheme S1). The stoichiometric reduction of 1Ti with 2 equiv of reductant generates yellow [ $K_2$ (THF) $_4$ Ti $_2$ L $_2$ ] ( $K_2$ -1Ti), while dark brown [ $K_4$ (THF) $_4$ Ti $_2$ (L $_2$ -) $_2$ ]  $K_4$ -1Ti can be made from careful reoxidation of  $K_6$ -1Ti (see the supplemental information). The solid-state structure of [ $K_4$ (THF) $_4$ Zr $_2$ (L $_2$ -) $_2$ ]  $K_4$ -1Zr is also shown in the supplemental information.

The reduced mixtures are active precatalysts for the  $N_2RR$  reactions and give similar product yields (Table S3, entries 1–4), although they may not be on-cycle intermediates according to the calculations described below. However, the metallated complexes  $K_n$ -1Ti (n = 4, 6) can become catalytically active upon the addition of weak acid, which reprotonates the benzylic C in  $K_n$ -1Ti (n = 4, 6).

The N–N bond orders of the two reduced  $N_2$  complexes were determined by Raman spectroscopy. Spectra of the 2Sm mixture contain an absorption at 1,337 cm<sup>-1</sup>, which is shifted to a lower energy (1,306 cm<sup>-1</sup>) for <sup>15</sup>N-2Sm, consistent with a doubly reduced  $N_2$  with a double-bond character (Figures S61–S63). Raman spectroscopy of 2Ti shows

#### Article



the presence of an N–N single bond. The absorption at  $v(^{15}N_2) = 796 \text{ cm}^{-1}$  in the Raman spectrum of the mixture reduced under  $^{15}N_2$ ,  $^{15}N$ -2Ti, shows a bathochromic shift compared to 2Ti ( $v(^{14}N_2) = 846 \text{ cm}^{-1}$ ) (Figures S65–S67). The shift is larger than predicted by the reduced mass calculation for the two N isotopes, which would be consistent with the involvement of the adjacent heavy atoms in this stretching mode. No N–H bonds were identified in 2Sm or 2Ti by Fourier transform infrared spectroscopy. Addition of weak acid to either  $^{15}N$ -2Sm or  $^{15}N$ -2Ti also generates a doublet in the  $^{1}H$  NMR spectrum at 7.35 ppm ( $^{1}J_{NH} = 71.3 \text{ Hz}$ ) indicative of  $^{15}NH_4CI$ , confirming that the amine N is derived from N<sub>2</sub> (Figures S28 and S33).

We were able to separate the other paramagnetic Ti complexes,  $K_2$ -1Ti and  $K_6$ -1Ti, from the 2Ti mixture by fractional crystallization. We then used pulsed electron paramagnetic resonance (EPR) spectroscopy to probe the remaining N<sub>2</sub>-bonded titanium species, denoted 1Ti-N<sub>2</sub>, and its isotopomer 1Ti-<sup>15</sup>N<sub>2</sub>. Q-band electron spin-echo modulation (ESEEM) spectra are shown in Figure 2. Very interestingly, while the majority of the modulation patterns in the 3-pulse ESEEM spectra arise from coupling to <sup>39</sup>K, a comparison between the frequency domain spectra of 1Ti-N<sub>2</sub> and 1Ti-<sup>15</sup>N<sub>2</sub> shows a sharp difference peak at 5.36 MHz, exactly at the Larmor frequency of <sup>15</sup>N at the Q-band (1,241 mT). The coupling to <sup>15</sup>N is corroborated by the two-dimensional hyperfine sublevel correlation spectroscopy, which clearly reveals a  $^{15}N$  coupling peak with a very small hyperfine interaction of  $\sim 0.2$  MHz, which likely arises from pure through-space electron nuclear dipole interactions, the magnitude of which implies very little, if any, orbital overlap between Ti<sup>III</sup> and  $^{15}$ N. Assuming a small T of 0.1–0.2 MHz corresponds to a Ti–N distance of 3–4 Å, which suggests that there is little or no covalency in the Ti-N2 bonding in 1Ti-N<sub>2</sub>. 43 Given the Ti<sup>III</sup>-Ti<sup>III</sup> distance of 6.36 Å calculated from the EPR spectra (seesupplemental information section 13) and the estimated N-N bond length of 1.2-1.4 Å, the Ti–N distance suggested by EPR for 1Ti-N<sub>2</sub> is estimated to be  $\sim$ 3.3 Å. Together, these data are consistent with a reduced N2 unit positioned in the center of the ligand cavity oriented in a side-on fashion relative to the two Ti centers.

EPR spectra of frozen 2-Me-THF solutions of several independently synthesized samples of 2Sm at 15 K show only a resonance assigned to an organic radical impurity at q = 2.005 without any discernable hyperfine features (Figure S73).

Because isolation of a highly reduced  $N_2$ -containing compound proved difficult, we carried out reactions targeted to trap the reduced  $N_2$  anion in 2Sm and 2Ti with various electrophiles (e.g., alkyl halides, phenyl isocyanate, and stoichiometric  $Me_3SiCl$ ) (see supplemental information section 6). Comparison of  $^1H$  NMR spectra between reactants and products showed subtle shifts in complex ligand resonances, but structural characterization of these products by XRD failed under numerous crystallization conditions.

#### **DISCUSSION**

#### Selectivity for secondary amine

This is the second report of catalytic  $N_2$  reduction providing a selective route to secondary amine product formation, following our identification of the  $U_2(L)_2$  catalyst 1U. To the best of our knowledge, all other systems reported to date make trisubstituted amines in the presence of CISiMe<sub>3</sub> except for Hidai's *cis*-Mo( $N_2$ )<sub>2</sub> (PMe<sub>2</sub>Ph)<sub>4</sub> complex, which catalytically converts  $N_2$  into mixtures of silylamines in up to 25.5 combined equiv per Mo; the best selectivity they could achieve for the bis(silyl)amine was at lower conversions, with excess  $N_2$  metal and  $N_2$  BrSiMe<sub>3</sub>,



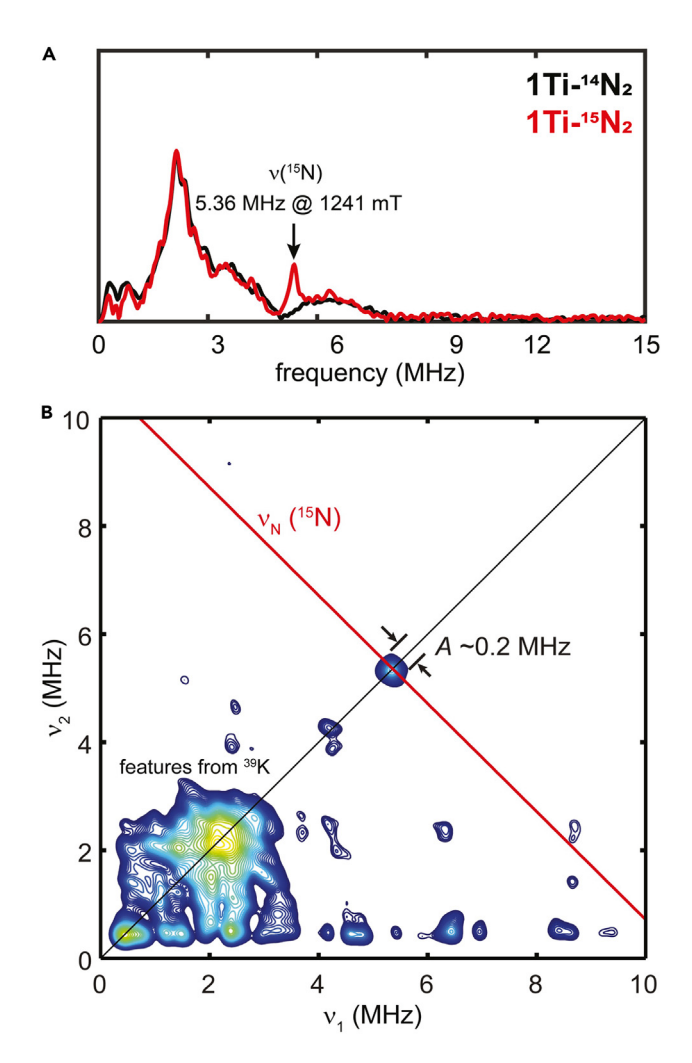


Figure 2. Pulsed EPR spectra of the isolated product of reduction of 1Ti under dinitrogen Q-band frequency domain 3-pulse ESEEM spectra of the isolated product of reduction of 1Ti under dinitrogen of (A) 1Ti- $N_2$  (black trace) and 1Ti- $^{15}N_2$  (red trace) reveal a difference peak at 5.36 MHz, exactly at the Larmor frequency for  $^{15}N$  at Q-band (1,241 mT). Q-band hyperfine sublevel correlation spectroscopy (HYSCORE) spectrum (B) of 1Ti- $^{15}N_2$  reveals the magnitude of the hyperfine coupling interaction of  $^{15}N$  and Ti<sup>III</sup> to be  $\sim$ 0.2 MHz. T = 20 K,  $\pi$ /2 = 12 ns,  $\tau$  = 300 ns.

converting  $N_2$  to a mixture of HN(SiMe<sub>3</sub>)<sub>2</sub> (1.8 mol/Mo atom) and N(SiMe<sub>3</sub>)<sub>3</sub> (3.2 mol/Mo atom). <sup>44</sup> The protons were suggested to derive from THF or trace water. Relatedly, Sita devised a stoichiometric route to HN(SiMe<sub>3</sub>)<sub>2</sub> by functionalizing a terminal Mo imido with sequential additions of acid, electrophile, and reductant. <sup>45</sup> Here, the pseudo-tetrahedrally coordinated 1Ti/Zr, like the unsolvated  $U_2(L)_2$  catalyst we previously reported, catalyze the synthesis of bis(silyl)amine but are inactive for the catalyzed formation of tris(silyl)amine. All these unsolvated complexes have smaller metallacyclic cavities than 1-Ln-THF, suggesting that the selective formation of bis(silyl) amine is most effectively controlled by the size of the metallacyclic pocket.

The 1Ln-THF precatalysts have pseudo-octahedral, THF-solvated metal cations (as does 1U-THF), large metallacyclic cavities, and presumably relatively flexible coordination geometries. They can catalyze the formation of bis(silyl)amine in the presence of silyl electrophile and acid but, in the absence of acid, can also catalyze the formation of tris(silyl)amine.

Article



Above, we noted that all four benzylic H point into the cavity for 1Ln-THF and 1M (Ln = Ce, Sm; M = Ti, Zr); tetra-dehydrometallation takes the complex off cycle as  $K_6$ -1M. The geometries of 1U and 1U-THF only allow for double dehydrometallation, leaving space for  $N_2$  binding in the cavity. Reprotonation of the tetra-dehydrometallated  $K_6$ -1M complexes brings them back on cycle, corroborating the calculations that find that the reaction takes place inside the cavity for Ti and U.

The kinetic studies of 1Ti, 1U-THF, and  $Ti(OAr)_4$  all confirm that  $HN(SiMe_3)_2$  is the dominant initial product of these aryloxide-supported electropositive-metal-mediated  $N_2RRs$ , and secondary reactions lead to tris(silyl)amine. Combined with the fact that neither 1Ti nor unsolvated 1U is able to produce the larger  $N(SiMe_3)_3$  catalytically, we reason that the small cavity space dominates the control of selectivity for the formation of the bis(silyl)amine product, while the  $R_3Si^+:H^+$  ratio influences the final product distribution. We have probed the latter by allowing a catalytic reaction involving 1Ti to stir for a longer time period (3 days) and observed higher yields of tris(silyl)amine at the expense of bis(silyl)amine (Table S2, entry 3).

### Identity of the Ln or group 4 metal and cooperativity with the group 1 metal reductant

The  $Ln^{III}$  and  $M^{IV}$  metallacycles 1 all feature the stable metal oxidation state and strong Ln/M–O bonding that characterized 1U, and again, there is no evidence of  $N_2$  binding until the reductant is added.

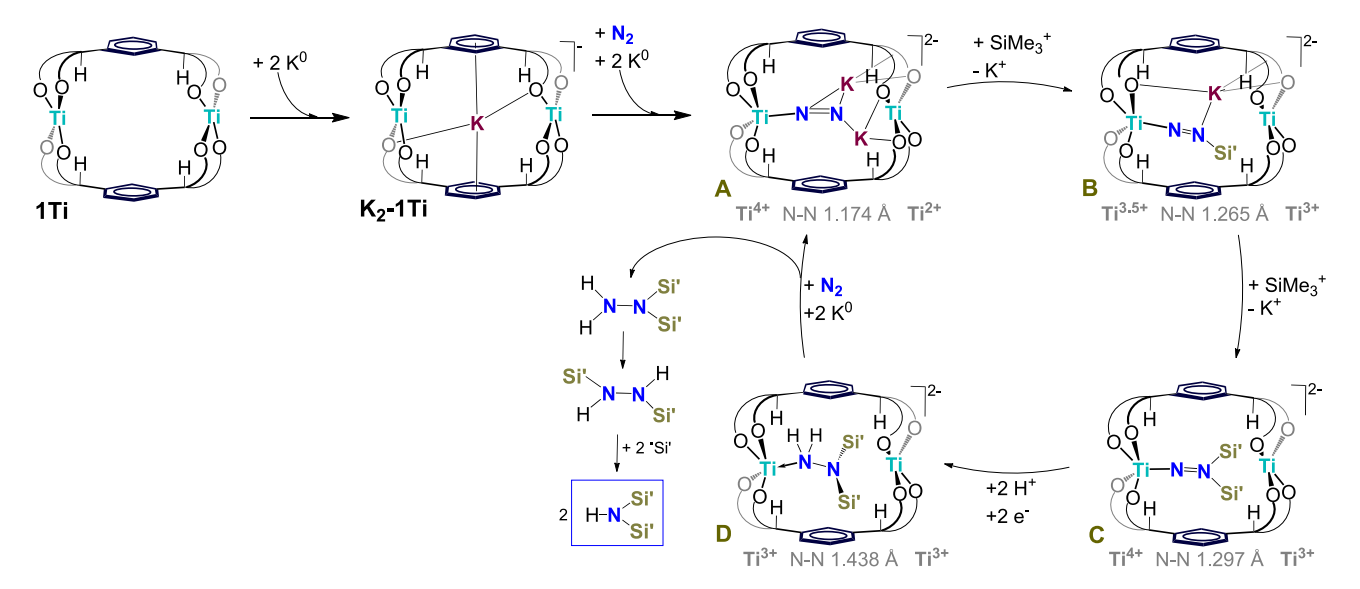
The group 4 complexes that do not bind donor solvents ( $r_{cov, 4-coord}$ : Ti(IV) = 0.56, Zr(IV) = 0.73 Å) and the unsolvated 1U can only form the smaller bis(silyl)amine product. The solvated 1Ln-THF and 1U-THF have a larger and likely more flexible metallacyclic cavity ( $r_{cov, 6-coord}$ : Ce(III) = 1.15 Å, Sm(III) = 1.098, U(IV) = 1.03 Å) and can catalyze the formation of either bis- or tris(silyl)amine.

Complex 1Ti can be reversibly reduced twice at  $E_{1/2}=-1.91\ V$  and  $-2.11\ V$  vs. Fc/Fc<sup>+</sup>, whereas no reduction event for 1Ln-THF, 1U-THF, and 1Zr that could be assigned to a metal reduction was measurable as far as  $-3.2\ V$  vs. Fc/Fc<sup>+</sup>. The values measured for 1Ti are very negative for a Ti<sup>IV/III</sup> couple, in line with the strongly electron-donating nature of the ligand set. In line with this observation, group 4 metal-locene complexes that reductively functionalize  $N_2^{46-48}$  did not show catalytic turn-over, perhaps because the cyclopentadienyl ligands do not support a sufficiently reducing metal center. <sup>49</sup> The higher reactivities for the Ti, Sm, and U catalysts, compared to their Zr, Ce, and Th<sup>19</sup> congeners, respectively, suggest that access to the reducing Ti<sup>IV/III</sup>, Sm<sup>III/II</sup>, and U<sup>IV/III50,51</sup> redox states, respectively, may be advantageous in  $N_2$ RR even if the binding mode of the reduced  $N_2$  intermediates is different in these different metal catalysts. <sup>52</sup>

Finally, the identity of the group 1 reductant is very important. Incorporation of the reductant counter cations is found to be essential in the calculated mechanism, providing electrostatic stabilization to intermediates, and was also shown to be essential for 1U.  $^{19}$  Various groups have noted the importance of group 1 countercation choice when stabilizing reduced  $\rm N_2$  complexes,  $^{53-55}$  If the first reduction potential of the Lewis acidic metal Ln  $^{\rm III/II}$  or  $\rm M^{\rm IV/III}$  in the metallacycle is less negative than the  $\rm M^{\rm O/I}$  potential of the reductant, then catalytic  $\rm N_2$  reduction is better. The  $\rm M^{\rm O/I}$  potential for Na is -2.56 V and for K and Rb is -2.88 V vs.  $\rm Fc^{\rm O/+}$  in MeCN.  $^{56}$  It is not clear why K is a better reductant partner for 1Sm-THF while Rb is a better partner for 1Ce-THF, but this could be due to a better fit of the s-block cations within the cavity that helps stabilize the reduced intermediates. The inability of the smaller,



# Chem Catalysis Article



Scheme 4. DFT-calculated structures of catalytic intermediates in the 1Ti cycle

The intermediates found by theory are shown as simplified cartoon line drawings, with the charges and redox states drawn underneath as found from the calculations.  $Si' = SiMe_3$ .

harder sodium to function as an effective reductant supports this, although there may be more of a redox potential difference between K and Rb in THF.

The most highly reduced, metalated complexes such as  $N_2$ -containing  $1\text{Sm-N}_2$  and  $1\text{Ti-N}_2$  are off cycle, while dehydrometallated  $K_4$ -1M and  $K_6$ -1M, which are formed from overreduction prior to  $N_2$  binding and have the smallest cavities, are not involved in the catalysis. Nevertheless, 2Ln and 2Ti are active precatalysts, and  $K_4$ -1Ti and  $K_6$ -1Ti can both reform  $K_2$ -1Ti and re-enter the  $N_2$ RR cycle.

### Proposed mechanism for 1Ti and comparison with possible mechanisms for 1Ln and 1An

Density functional theory (DFT) calculations were undertaken to identify possible reaction intermediates for an N<sub>2</sub>RR catalytic cycle mediated by 1Ti, and the structures of theoretical catalytic intermediates are shown in Scheme 4. The methods used mirrored those for the 1U system, but we have found that, computationally, the 3d and 5f compounds behave differently. The lack of formation of any bis(silylamine) by 1Ln-THF catalysts in the absence of weak acid also implies mechanistic differences between 1Ln-THF and 1U. The side-on N<sub>2</sub> arrangement from the U modeling was initially used for the Ti calculations, but numerous attempts at getting  $N_2$  reduction in this configuration were unsuccessful (vide infra). End-on-bound N2 is more reactive toward further functionalization than side-on-bound N<sub>2</sub> in reported d-block chemistry.<sup>57</sup> Further, reduced U pathways were not previously considered for U, as it was not necessary to do so. The U mechanism calculations focused on transformations between intermediates in which K cations were replaced by silyl cations and did not consider the potential role of SiMe<sub>3</sub> radicals. While others suggest that the Me<sub>3</sub>Si· radical may be involved in solution-phase catalytic N<sub>2</sub>RR at low temperatures (150–200 K), the Me<sub>3</sub>Si· radical has a half-life of 0.005–0.01 s. $^{58}$ 

We begin with 1Ti modeled as a neutral singlet with two Ti(IV) centers. Calculation gives Ti–Ti = 7.813 Å and average Ti–O = 1.808 Å, which compare well with the experimental values of 7.890 and 1.812 Å, respectively. From 1Ti, we move to  $K_2$ -

Article



1Ti, here modeled as a monoanionic triplet with only the internal K cation present and the external counter cation excluded from the calculation. The structural agreement with experiment is once again very good: calculated Ti-Ti = 7.728 Å, Ti-K = 3.864 Å, and average Ti-O = 1.913 Å vs. 7.676, 3.838, and 1.914 Å from XRD. The Mulliken spin density is 1.029 on each Ti(III) center. At this stage, we introduce an additional K and an N<sub>2</sub> molecule. The latter was initially placed in a variety of starting orientations, midway between the two Ti centers, and with overall  $C_i$  symmetry. Subsequent symmetry-constrained geometry optimizations of systems with different spin multiplicities yielded little evidence of  $N_2$  reduction, with N-N distances close to those in free dinitrogen. Harmonic vibrational frequency analysis indicated that one of the converged geometries—a quintet in which the N<sub>2</sub> unit is oriented approximately along the Ti-Ti vector—is a transition state, with an imaginary mode of 69.2i cm<sup>-1</sup> corresponding to translation of the N<sub>2</sub> unit between the Ti centers. Relaxed geometry optimization yielded a structure that is 67.3 kJ/mol more stable in energy than the transition state, in which the N<sub>2</sub> unit bonds to only one of the Ti centers and the N-N distance lengthens to 1.172 Å.

Subsequent reoptimization of this system in different spin states established that the most stable structure is a triplet, 46.5 kJ/mol more stable than the quintet, and with a very similar geometry (N-N = 1.174 Å, Ti-N = 1.901 Å) (intermediate A in Scheme 4). The spin-density data suggest that the N2-bound Ti is Ti(IV), with minimal spin density on the  $N_2$  unit. The other Ti center has spin density = 1.929. We were surprised to find that one Ti center plays the dominant role because almost all electropositive metal complexes containing reductively functionalized N2 reported to date contain the reduced  $N_2$  anion bound to two metals, and all of these are symmetrical.<sup>21</sup> However, we note that only 1Ti and the two tren-supported complexes cited above 16,17 have shown N<sub>2</sub>RR catalysis. Moreover, the distal mechanism, which invokes end-on binding and would seem most reasonable for Ti(OAr)4, is more common for those catalysts whose mechanisms have been studied so far.<sup>57</sup> Note also that while the computed mechanism for N<sub>2</sub> reduction by our uranium-based catalyst<sup>19</sup> featured side-on-bound N<sub>2</sub> coordinated by both metals, the U-U distance in the precatalyst 1U is  $\sim$ 1.3 Å shorter than the Ti–Ti distance in 1Ti (which also features significantly smaller metal ions). Upon reductive activation of dinitrogen by 1U, the U-U distance decreases by 1.931  $\mathring{A}$ . <sup>19</sup> A molecule of  $N_2$  placed centrally in an end-on geometry in the cavity of the Sm<sup>III</sup> starting material 1Sm-THF would have an Sm-N distance of 4.13 Å, which is too long for any significant orbital overlap, but the mechanism calculated for 1Ti shows N<sub>2</sub> binding to only one Ti during catalysis, and group 1 metal cations fill the remaining space before being replaced by electrophiles. There appears to be only a minimal energy difference between the side-on- and end-onbound (N2)2- isomers in the instances where both have been reported for  $\{X_2Ln(sol)_n\}_2(\mu-N_2).^{26-34}$ 

From A we move to species B, in which one of the K ions bound to the distal N is replaced by  $SiMe_3^+$ . This system, as with all the others shown in Scheme 4 except 1Ti and  $K_2$ -1Ti, is a dianionic triplet. The spin density is distributed such that the  $N_2$ -free Ti is Ti(III), with the residual spin spread over the other Ti (0.363) and the  $N_2$  unit (0.538). The buildup of spin density on the latter is consistent with the lengthening of the N–N distance to 1.265 Å in a formal  $[KSiMe_3N_2]^{-0.5}$  group. Replacement of the second N-bound  $K^+$  with  $SiMe_3^+$  leads to species C, in which there is greater spin-density buildup on the  $N_2$  (0.702) and an even longer N–N (1.297 Å). The  $N_2$ -free Ti remains Ti(III), and the Ti– $N_2$  distance remains short at 1.770 Å.



The final structure we have located is D. Two hydrogen atoms are added to the proximal N, leading to substantial changes in the spin-density distribution and key distances. Both Ti centers are now Ti(III), and the  $N_2$  unit now carries almost no net spin density. This is consistent with further lengthening of the N–N distance to 1.438 Å and an N–N single bond. The Ti– $N_2$  distance also lengthens substantially and at 2.116 Å is now 0.346 Å longer than in C. The overall structure of D is essentially a doubly reduced version of 1Ti with an  $H_2N_2(SiMe_3)_2$  molecule sitting in the cavity, and while intermediates with one silyl group on each nitrogen were also investigated computationally, the Ti cavity limits silylation to two per  $N_2$ .

Release of the disilylhydrazine bound inside the  $Ti_2L_2$  cavity (Scheme 4) is easy, and the 1,2 rearrangement of silylalkyl groups in disilylhydrazine is known to be rapid, so upon release from the cavity,  $HNNSi'_2$  rapidly forms the more stable 1,2-disilylhydrazine (Z),<sup>59</sup> which can react with the excess  $\cdot SiMe_3$  radicals<sup>60,61</sup> to form the  $HN(SiMe_3)_2$  product.

We have combined the DFT-calculated proposed mechanism for 1Ti with the observations made for 1Ln-THF and 1U(-THF) in Scheme S1.

#### **Conclusions**

Metallacyclic group 4 and f-block complexes of tetradentate, bridging aryloxides, are capable of binding dinitrogen in the cavity formed by the chelating aryloxide ligands upon reduction. The complexes demonstrate selective catalytic functionalization of dinitrogen to secondary amines by the rare earths and zirconium, a product yet to be made catalytically by all the other d-block catalysts to date. The group 4 complexes selectively make the secondary amine in yields of up to 84.1 equiv per complex, while the more coordinatively flexible f-block complexes can catalyze the  $N_2RR$  to make either  $HN(SiMe_3)_2$  or  $N(SiMe_3)_3$  amines from atmospheric dinitrogen in yields of up to 6.4 and 7.8 equiv per complex, respectively.

Kinetic and computational studies show that the bis(silyl)amine is the favored product when weak acid and trimethylsilyl electrophile are present. The ligand framework also helps to accommodate the group 1 counter cations needed to stabilize the reduced  $N_2$ -containing intermediates. DFT calculations on the titanium-catalyzed reaction find that the major functionalization steps are associated with  $N_2$  adopting an end-on binding to just one of the metal centers, with the reducing group 1 alkali cations, rather than the second metal, stabilizing the distal N. This mechanism, involving the reduction of at least one metal in all the located intermediates, differs from the side-on mechanism reported by Arnold et al. <sup>19</sup> in which reduction to U(III) was not considered or required. Further work is in progress to determine the nature of  $N_2$  binding in the intermediates in the lanthanide-catalyzed reactions and if reduced f-block metal centers can play a role in the catalysis.

The  $N_2RR$  catalysis by 1Zr is the first example of  $N_2RR$  for a zirconium complex to our knowledge. Differences in the reactivity of the group 4, lanthanide, and actinide metallacycles, coupled with theory, suggest that the  $N_2$  coordination to electropositive metal cations that are easier to reduce enables sufficient activation of the bound  $N_2$  in the cavity such that it can be functionalized. Furthermore, the metallacycles with smaller cavities, 1Ti, 1Zr, and unsolvated 1U, make secondary silylamines, while the solvated Ln and Ln systems with larger cavities, Ln-THF and Ln-THF, make secondary or tertiary amines depending on the reagents. The differences between Ln-RD as reductants show the importance of the choice of group Ln-THF and in dinitrogen reduction chemistry.



In addition to demonstrating N<sub>2</sub>RR catalysis with the most abundant lanthanides, the formation of secondary amines using plentiful titanium under ambient conditions is notable. The ability to function in polar solvents suggests that the chemical reductant in these reactions could be replaced by a greener electrochemical source of electrons in the future. 62,63

#### **EXPERIMENTAL PROCEDURES**

#### Resource availability

#### Lead contact

Requests for further information and resources should be directed to and will be fulfilled by the lead contact, Polly L. Arnold (pla@berkeley.edu).

#### Materials availability

The catalysts described are available upon request, but we might require a payment because of their need to be synthesized by researchers with suitable expertise in an appropriate facility.

#### Data and code availability

Crystallographic data in CIF format are available at https://ccdc.cam.ac.uk/ under accession codes CCDC: 2181896-2181898, 2195247 and 2204194, 2210077-2210079, 2210081-2210083, and 2307225. Raw datasets for all other processed data in this paper are available at https://doi.org/10.5061/dryad.3r2280gpz. Full synthetic and characterization data for the compounds and catalysts described are available in the supplemental information. Computational details and xyz coordinates of the computed intermediates are provided in Scheme 4.

#### SUPPLEMENTAL INFORMATION

Supplemental information can be found online at https://doi.org/10.1016/j.checat. 2024.100964.

#### **ACKNOWLEDGMENTS**

The synthetic work was supported by the National Science Foundation (CHE-2154369 to A.W. and P.L.A.) and the US Department of Energy (DOE) Office of Science, Office of Basic Energy Sciences, Chemical Sciences, Geosciences, and Biosciences Division in the Catalysis Program (J.L., M.H., and A.W.) and the Rare Earth Project in the Separations Program at the Lawrence Berkeley National Laboratory (F.Y.T.L., T.M.T., and P.L.A.). The Catalysis Laboratory in the DOE Catalysis Program also provided resources and instrumentation used in this work, and some diffraction data were collected at Beamline 12.2.1 of the Advanced Light Source, which is a DOE Office of Science User Facility. All of these DOE programs and facilities operate under contract no. DE-AC02-05CH11231. EPR spectroscopic studies were funded by the National Institutes of Health (NIH) (R35 grant 1R35GM126961 to R.D.B.). Raman spectra were acquired on instrumentation provided by the Liquid Sunlight Alliance, which is supported by the US DOE Office of Science, Office of Basic Energy Sciences, Fuels from Sunlight Hub, under award no. DE-SC0021266. Funding for CheXray comes from an NIH Shared Instrument Grant (S10-RR027172). We thank Hasan Celik for NMR spectroscopic support and discussions and the NIH for funding the UC Berkeley College of Chemistry NMR facility under grant no. 1S10RR016634-01. We thank The University of Manchester for its Computational Shared Facility (CSF3 and CSF4) and associated support services. We also thank the UK EPSRC for financial support through grant number EP/X042049/1. This project also received funding for some of the early synthetic work from the European Research



Council under the European Union's Horizon 2020 Research and Innovation Programme (grant agreement no. 740311 to P.L.A. and R.P.K.). We thank Amy Kynman for the graphical abstract artwork.

#### **AUTHOR CONTRIBUTIONS**

A.W., F.Y.T.L., M.H., J.L., T.M.T., R.P.K., and T.O. made and characterized the compounds and reactions and, with P.L.A., analyzed the data and wrote the manuscript. G.R. and R.D.B. collected and interpreted the EPR spectra. N.K. carried out and analyzed the mechanistic calculations and wrote the DFT part of the manuscript. P.L.A. raised the funding and conceptualized the project with contributions from A.W., F.Y.T.L., R.D.B., and N.K., and all authors reviewed and edited the manuscript. F.Y.T.L., M.H., and J.L. contributed equally.

#### **DECLARATION OF INTERESTS**

An international patent application (PCT/US23/74839) has been filed with the US receiving office.

Received: November 16, 2023 Revised: February 11, 2024 Accepted: March 13, 2024 Published: April 8, 2024

#### **REFERENCES**

- Kuriyama, S., and Nishibayashi, Y. (2021). Development of catalytic nitrogen fixation using transition metal complexes not relevant to nitrogenases. Tetrahedron 83, 131986. https://doi.org/10.1016/j.tet.2021.131986.
- Yandulov, D.V., and Schrock, R.R. (2003). Catalytic reduction of dinitrogen to ammonia at a single molybdenum center. Science 301, 76–78. https://doi.org/10.1126/science. 1085326.
- Sekiguchi, Y., Arashiba, K., Tanaka, H., Eizawa, A., Nakajima, K., Yoshizawa, K., and Nishibayashi, Y. (2018). Catalytic Reduction of Molecular Dinitrogen to Ammonia and Hydrazine Using Vanadium Complexes. Angew. Chem. Int. Ed. 57, 9064–9068. https:// doi.org/10.1002/anie.201802310.
- Yin, J., Li, J., Wang, G.-X., Yin, Z.-B., Zhang, W.-X., and Xi, Z. (2019). Dinitrogen Functionalization Affording Chromium Hydrazido Complex. J. Am. Chem. Soc. 141, 4241–4247. https://doi.org/10.1021/jacs. 9b00822.
- Anderson, J.S., Rittle, J., and Peters, J.C. (2013). Catalytic conversion of nitrogen to ammonia by an iron model complex. Nature 501, 84–87. https://doi.org/10.1038/ nature12435.
- Piascik, A.D., Li, R., Wilkinson, H.J., Green, J.C., and Ashley, A.E. (2018). Fe-Catalyzed Conversion of N2 to N(SiMe3)3 via an Fe-Hydrazido Resting State. J. Am. Chem. Soc. 140, 10691–10694. https://doi.org/10.1021/ iacs.8h06999
- 7. Fajardo, J., Jr., and Peters, J.C. (2017). Catalytic Nitrogen-to-Ammonia Conversion by Osmium and Ruthenium Complexes. J. Am. Chem. Soc.

- 139, 16105–16108. https://doi.org/10.1021/jacs.7b10204.
- Ashida, Y., Mizushima, T., Arashiba, K., Egi, A., Tanaka, H., Yoshizawa, K., and Nishibayashi, Y. (2023). Catalytic production of ammonia from dinitrogen employing molybdenum complexes bearing N-heterocyclic carbenebased PCP-type pincer ligands. Nat. Synth. 2, 635–644. https://doi.org/10.1038/s44160-023-00292-9.
- Arashiba, K., Miyake, Y., and Nishibayashi, Y. (2011). A molybdenum complex bearing PNPtype pincer ligands leads to the catalytic reduction of dinitrogen into ammonia. Nat. Chem. 3, 120–125. https://doi.org/10.1038/ pspen 206.
- Tanaka, H., Arashiba, K., Kuriyama, S., Sasada, A., Nakajima, K., Yoshizawa, K., and Nishibayashi, Y. (2014). Unique behaviour of dinitrogen-bridged dimolybdenum complexes bearing pincer ligand towards catalytic formation of ammonia. Nat. Commun. 5, 3737. https://doi.org/10.1038/ncomms4737.
- Arashiba, K., Kinoshita, E., Kuriyama, S., Eizawa, A., Nakajima, K., Tanaka, H., Yoshizawa, K., and Nishibayashi, Y. (2015). Catalytic Reduction of Dinitrogen to Ammonia by Use of Molybdenum-Nitride Complexes Bearing a Tridentate Triphosphine as Catalysts. J. Am. Chem. Soc. 137, 5666–5669. https://doi.org/10. 1021/jacs.5b02579.
- Eizawa, A., Arashiba, K., Tanaka, H., Kuriyama, S., Matsuo, Y., Nakajima, K., Yoshizawa, K., and Nishibayashi, Y. (2017). Remarkable catalytic activity of dinitrogen-bridged dimolybdenum complexes bearing NHC-based PCP-pincer ligands toward nitrogen fixation. Nat. Commun. 8, 14874. https://doi.org/10.1038/ ncomms14874.

- Ashida, Y., Arashiba, K., Nakajima, K., and Nishibayashi, Y. (2019). Molybdenum-catalysed ammonia production with samarium diiodide and alcohols or water. Nature 568, 536–540. https://doi.org/10.1038/s41586-019-1134-2.
- Bora, D., Gayen, F.R., and Saha, B. (2022). Ammonia from dinitrogen at ambient conditions by organometallic catalysts. RSC Adv. 12, 33567–33583. https://doi.org/10.1039/ D2RA06156B.
- Huang, W., Peng, L.-Y., Zhang, J., Liu, C., Song, G., Su, J.-H., Fang, W.-H., Cui, G., and Hu, S. (2023). Vanadium-Catalyzed Dinitrogen Reduction to Ammonia via a [V] NNH<sub>2</sub> Intermediate. J. Am. Chem. Soc. 145, 811–821. https://doi.org/10.1021/jacs.2c08000.
- Doyle, L.R., Wooles, A.J., Jenkins, L.C., Tuna, F., McInnes, E.J.L., and Liddle, S.T. (2018). Catalytic Dinitrogen Reduction to Ammonia at a Triamidoamine–Titanium Complex. Angew. Chem. Int. Ed. 57, 6314–6318. https://doi.org/ 10.1002/anie.201802576.
- Ghana, P., van Krüchten, F.D., Spaniol, T.P., van Leusen, J., Kögerler, P., and Okuda, J. (2019). Conversion of dinitrogen to tris(trimethylsilyl) amine catalyzed by titanium triamido-amine complexes. Chem. Commun. 55, 3231–3234. https://doi.org/10.1039/C8CC09742A.
- Sekiguchi, Y., Meng, F., Tanaka, H., Eizawa, A., Arashiba, K., Nakajima, K., Yoshizawa, K., and Nishibayashi, Y. (2018). Synthesis and reactivity of titanium- and zirconium-dinitrogen complexes bearing anionic pyrrole-based PNP-type pincer ligands. Dalton Trans. 47, 11322–11326. https://doi.org/10.1039/ C8DT02739K.
- 19. Arnold, P.L., Ochiai, T., Lam, F.Y.T., Kelly, R.P., Seymour, M.L., and Maron, L. (2020).

#### **Article**



- Metallacyclic actinide catalysts for dinitrogen conversion to ammonia and secondary amines. Nat. Chem. 12, 654–659. https://doi.org/10.1038/s41557-020-0457-9.
- Wells, J.A.L., Seymour, M.L., Suvova, M., and Arnold, P.L. (2016). Dinuclear uranium complexation and manipulation using robust tetraaryloxides. Dalton Trans. 45, 16026–16032. https://doi.org/10.1039/C6DT02630C.
- Mansell, S.M., Kaltsoyannis, N., and Arnold, P.L. (2011). Small Molecule Activation by Uranium Tris(aryloxides): Experimental and Computational Studies of Binding of N<sub>2</sub>, Coupling of CO, and Deoxygenation Insertion of CO<sub>2</sub> under Ambient Conditions. J. Am. Chem. Soc. 133, 9036–9051. https://doi.org/10. 1021/ja2019492.
- Mansell, S.M., Farnaby, J.H., Germeroth, A.I., and Arnold, P.L. (2013). Thermally stable uranium dinitrogen complex with siloxide supporting ligands. Organometallics 32, 4214– 4222. https://doi.org/10.1021/om4003957.
- Batov, M.S., del Rosal, I., Scopelliti, R., Fadaei-Tirani, F., Zivkovic, I., Maron, L., and Mazzanti, M. (2023). Multimetallic Uranium Nitride Cubane Clusters from Dinitrogen Cleavage. J. Am. Chem. Soc. 145, 26435–26443. https:// doi.org/10.1021/jacs.3c10617.
- Hasanayn, F., Holland, P.L., Goldman, A.S., and Miller, A.J.M. (2023). Lewis Structures and the Bonding Classification of End-on Bridging Dinitrogen Transition Metal Complexes. J. Am. Chem. Soc. 145, 4326–4342. https://doi.org/10. 1021/jacs.2c12243.
- Evans, W.J., Ulibarri, T.A., and Ziller, J.W. (1988). Isolation and x-ray crystal structure of the first dinitrogen complex of an f-element metal, [(C<sub>5</sub>Me<sub>5</sub>)<sub>2</sub>Sm]<sub>2</sub>N<sub>2</sub>. J. Am. Chem. Soc. 110, 6877–6879. https://doi.org/10.1021/ja00228a043.
- Turner, Z. (2015). Molecular pnictogen activation by rare earth and actinide complexes. Inorganics 3, 597–635.
- Evans, W.J., and Lee, D.S. (2005). Early developments in lanthanide-based dinitrogen reduction chemistry. Can. J. Chem. 83, 375–384. https://doi.org/10.1139/v05-014.
- Evans, W.J., Rego, D.B., and Ziller, J.W. (2006). Synthesis, structure, and <sup>15</sup>N NMR studies of paramagnetic lanthanide complexes obtained by reduction of dinitrogen. Inorg. Chem. 45, 10790–10798. https://doi.org/10.1021/ ic061485g.
- 29. Evans, W.J., Lorenz, S.E., and Ziller, J.W. (2009). Investigating metal size effects in the  $\text{Ln}_2(\mu \eta^2:\eta^2-N_2)$  reduction system: Reductive reactivity with complexes of the largest and smallest trivalent lanthanide ions,  $\text{La}^{3+}$  and  $\text{Lu}^{3+}$ . Inorg. Chem. 48, 2001–2009. https://doi.org/10.1021/ic801853d.
- Rinehart, J.D., Fang, M., Evans, W.J., and Long, J.R. (2011). A N<sub>2</sub><sup>3-</sup> Radical-Bridged Terbium Complex Exhibiting Magnetic Hysteresis at 14 K. J. Am. Chem. Soc. 133, 14236–14239. https://doi.org/10.1021/ja206286h.
- 31. MacDonald, M.R., Bates, J.E., Fieser, M.E., Ziller, J.W., Furche, F., and Evans, W.J. (2012). Expanding Rare-Earth Oxidation State Chemistry to Molecular Complexes of Holmium(II) and Erbium(II). J. Am. Chem. Soc.

- 134, 8420–8423. https://doi.org/10.1021/ja303357w.
- 32. Woen, D.H., Chen, G.P., Ziller, J.W., Boyle, T.J., Furche, F., and Evans, W.J. (2017). End-On Bridging Dinitrogen Complex of Scandium. J. Am. Chem. Soc. 139, 14861–14864. https:// doi.org/10.1021/jacs./b08456.
- 33. Ryan, A.J., Balasubramani, S.G., Ziller, J.W., Furche, F., and Evans, W.J. (2020). Formation of the end-on bound lanthanide dinitrogen complexes [(R<sub>2</sub>N)<sub>3</sub>Ln-N=N-Ln(NR<sub>2</sub>)<sub>3</sub>]<sup>2-</sup> from divalent [(RN)<sub>3</sub>Ln]<sup>1-</sup> salts (R = SiMe<sub>3</sub>). J. Am. Chem. Soc. 142, 9302–9313. https://doi.org/10.1021/jacs.0c01021.
- Mondal, A., Price, C.G.T., Tang, J., and Layfield, R.A. (2023). Targeted Synthesis of End-On Dinitrogen-Bridged Lanthanide Metallocenes and Their Reactivity as Divalent Synthons. J. Am. Chem. Soc. 145, 20121–20131. https://doi.org/10.1021/jacs.3c07600.
- 35. Fang, M., Bates, J.E., Lorenz, S.E., Lee, D.S., Rego, D.B., Ziller, J.W., Furche, F., and Evans, W.J. (2011). ( $N_2$ )<sub>3</sub>— Radical Chemistry via Trivalent Lanthanide Salt/Alkali Metal Reduction of Dinitrogen: New Syntheses and Examples of ( $N_2$ )<sup>2</sup>— and ( $N_2$ )<sup>3</sup>— Complexes and Density Functional Theory Comparisons of Closed Shell Sc<sup>3+</sup>, Y<sup>3+</sup>, and Lu<sup>3+</sup> versus 4f<sup>9</sup> Dy<sup>3+</sup>. Inorg. Chem. 50, 1459–1469. https://doi.org/10.1021/ic102016k.
- 36. Demir, S., Gonzalez, M.I., Darago, L.E., Evans, W.J., and Long, J.R. (2017). Giant coercivity and high magnetic blocking temperatures for N<sub>2</sub><sup>3-</sup> radical-bridged dilanthanide complexes upon ligand dissociation. Nat. Commun. 8, 2144. https://doi.org/10.1038/s41467-017-01553-w.
- Lv, Z.-J., Huang, Z., Zhang, W.-X., and Xi, Z. (2019). Scandium-Promoted Direct Conversion of Dinitrogen into Hydrazine Derivatives via N-C Bond Formation. J. Am. Chem. Soc. 141, 8773–8777. https://doi.org/10.1021/jacs.9b04293.
- Fang, M., Lee, D.S., Ziller, J.W., Doedens, R.J., Bates, J.E., Furche, F., and Evans, W.J. (2011). Synthesis of the (N<sub>2</sub>)<sup>3-</sup> Radical from Y<sup>2+</sup> and Its Protonolysis Reactivity To Form (N<sub>2</sub>H<sub>2</sub>)<sup>2-</sup> via the Y[N(SiMe<sub>3</sub>)<sub>2</sub>]<sub>3</sub>/KC<sub>8</sub> Reduction System. J. Am. Chem. Soc. 133, 3784–3787. https://doi. org/10.1021/ja1116827.
- Shephard, J.J., Berryman, V.E.J., Ochiai, T., Walter, O., Price, A.N., Warren, M.R., Arnold, P.L., Kaltsoyannis, N., and Parsons, S. (2022). Covalent bond shortening and distortion induced by pressurization of thorium, uranium, and neptunium tetrakis aryloxides. Nat. Commun. 13, 5923. https://doi.org/10.1038/ s41467-022-33459-7.
- Lateskey, S., Keddington, J., McMullen, A.K., Rothwell, I.P., and Huffman, J.C. (1985). Chemistry of sterically crowded aryloxide ligands. 5. Synthesis, structure, spectroscopic properties, and electrochemical behavior of group 4 metal derivatives containing bulky aryloxide ligands. Inorg. Chem. 24, 995–1001. https://doi.org/10.1021/ic00201a007.
- David, F.H. (2008). About low oxidation states, hydration and covalence properties of f elements. Radiochim. Acta 96, 135–144. https://doi.org/10.1524/ract.2008.1470.

- Evans, W.J. (2016). Tutorial on the role of cyclopentadienyl ligands in the discovery of molecular complexes of the rare-earth and actinide metals in new oxidation states. Organometallics 35, 3088–3100. https://doi. org/10.1021/acs.organomet.6b00466.
- Bae, D.Y., Lee, G., and Lee, E. (2021). Fixation of Dinitrogen at an Asymmetric Binuclear Titanium Complex. Inorg. Chem. 60, 12813– 12822. https://doi.org/10.1021/acs.inorgchem. 1c01050.
- Komori, K., Oshita, H., Mizobe, Y., and Hidai, M. (1989). Preparation and properties of molybdenum and tungsten dinitrogen complexes. 25. Catalytic conversion of molecular nitrogen into silylamines using molybdenum and tungsten dinitrogen complexes. J. Am. Chem. Soc. 111, 1939–1940. https://doi.org/10.1021/ja00187a092.
- 45. Duman, L.M., and Sita, L.R. (2017). Closing the Loop on Transition-Metal-Mediated Nitrogen Fixation: Chemoselective Production of HN(SiMe<sub>3</sub>)<sub>2</sub> from N<sub>2</sub>, Me<sub>3</sub>SiCl, and X—OH (X = R, R<sub>3</sub>Si, or Silica Gel). J. Am. Chem. Soc. 139, 17241–17244. https://doi.org/10.1021/jacs. 7b08859.
- Manriquez, J.M., and Bercaw, J.E. (1974). Preparation of a dinitrogen complex of bis(pentamethylcyclopentadienyl)zirconium(II). Isolation and protonation leading to stoichiometric reduction of dinitrogen to hydrazine. J. Am. Chem. Soc. 96, 6229–6230. https://doi.org/10.1021/ja00826a071.
- Knobloch, D.J., Lobkovsky, E., and Chirik, P.J. (2010). Dinitrogen cleavage and functionalization by carbon monoxide promoted by a hafnium complex. Nat. Chem. 2, 30–35. https://doi.org/10.1038/nchem.477.
- Kim, S., Loose, F., and Chirik, P.J. (2020). Beyond Ammonia: Nitrogen–Element Bond Forming Reactions with Coordinated Dinitrogen. Chem. Rev. 120, 5637–5681. https://doi.org/10.1021/acs.chemrev.9b00705.
- Hanna, T.E., Lobkovsky, E., and Chirik, P.J. (2009). Dinitrogen Complexes of Bis(cyclopentadienyl) Titanium Derivatives: Structural Diversity Arising from Substituent Manipulation. Organometallics 28, 4079–4088. https://doi.org/10.1021/om900282u.
- Bratsch, S.G., and Lagowski, J.J. (1985). Lanthanide thermodynamic predictions. 7. Thermodynamics of 2+, 3+, and 4+ aquo ions and standard electrode potentials at 298.15 K. J. Phys. Chem. 89, 3317–3319. https://doi.org/ 10.1021/j100261a031.
- Bratsch, S.G., and Lagowski, J.J. (1986). Actinide thermodynamic predictions. 3. Thermodynamics of compounds and aquoions of the 2+, 3+, and 4+ oxidation states and standard electrode potentials at 298.15 K. J. Phys. Chem. 90, 307–312. https://doi.org/10.1021/j100274a021.
- Kawaguchi, H., and Matsuo, T. (2004). Aryloxide-based multidentate ligands for early transition metals and f-element metals.
   J. Organomet. Chem. 689, 4228–4243. https:// doi.org/10.1016/j.jorganchem.2004.08.004.
- 53. Falcone, M., Chatelain, L., Scopelliti, R., Živković, I., and Mazzanti, M. (2017). Nitrogen reduction and functionalization by a



- multimetallic uranium nitride complex. Nature 547, 332–335. https://doi.org/10.1038/nature/3279.
- Suzuki, S., Ishida, Y., Kameo, H., Sakaki, S., and Kawaguchi, H. (2020). Counterion Dependence of Dinitrogen Activation and Functionalization by a Diniobium Hydride Anion. Angew. Chem. Int. Ed. 59, 13444–13450. https://doi.org/10. 1002/anie.202006039.
- Grubel, K., Brennessel, W.W., Mercado, B.Q., and Holland, P.L. (2014). Alkali Metal Control over N–N Cleavage in Iron Complexes. J. Am. Chem. Soc. 136, 16807–16816. https://doi.org/ 10.1021/ja507442b.
- Marcus, Y. (1985). Thermodynamic functions of transfer of single ions from water to nonaqueous and mixed solvents: Part 3 -Standard potentials of selected electrodes. Pure Appl. Chem. 57, 1129–1132. https://doi. org/10.1351/pac198557081129.

- 57. Lv, Z.-J., Wei, J., Zhang, W.-X., Chen, P., Deng, D., Shi, Z.-J., and Xi, Z. (2020). Direct transformation of dinitrogen: synthesis of N-containing organic compounds via N-C bond formation. Natl. Sci. Rev. 7, 1564–1583. https://doi.org/10.1093/nsr/nwaa142 %.
- Tumanskii, B., Karni, M., and Apeloig, Y. (2012). Persistent and Stable Silyl Radicals. In Encyclopedia of Radicals in Chemistry, Biology and Materials. https://doi.org/10.1002/ 9781119953678.rad066.
- West, R., Ishikawa, M., and Bailey, R.B. (1966). Anionic Rearrangement of Hydrazines. II.1 Isomers of Bis(organosilyl)hydrazines2. J. Am. Chem. Soc. 88, 4648–4652. https://doi.org/10. 1021/ja00972a022.
- Siedschlag, R.B., Bernales, V., Vogiatzis, K.D., Planas, N., Clouston, L.J., Bill, E., Gagliardi, L., and Lu, C.C. (2015). Catalytic silylation of dinitrogen with a dicobalt complex. J. Am.

- Chem. Soc. 137, 4638–4641. https://doi.org/10.1021/jacs.5b01445.
- Chalkley, M.J., Drover, M.W., and Peters, J.C. (2020). Catalytic N<sub>2</sub>-to-NH<sub>3</sub> (or -N<sub>2</sub>H<sub>4</sub>)
   Conversion by Well-Defined Molecular Coordination Complexes. Chem. Rev. 120, 5582–5636. https://doi.org/10.1021/acs.chemrev.9b00638.
- 62. Qing, G., Ghazfar, R., Jackowski, S.T., Habibzadeh, F., Ashtiani, M.M., Chen, C.-P., Smith, M.R., and Hamann, T.W. (2020). Recent Advances and Challenges of Electrocatalytic N<sub>2</sub> Reduction to Ammonia. Chem. Rev. 120, 5437–5516. https://doi.org/10.1021/acs. chemrev.9b00659.
- Garrido-Barros, P., Derosa, J., Chalkley, M.J., and Peters, J.C. (2022). Tandem electrocatalytic N<sub>2</sub> fixation via proton-coupled electron transfer. Nature 609, 71–76. https:// doi.org/10.1038/s41586-022-05011-6.